QUANTITATIVE ASSESSMENT OF THE RISK OF AIRBORNE TRANSMISSION OF SARS-CoV-2 INFECTION: PROSPECTIVE AND RETROSPECTIVE APPLICATIONS

G. Buonanno[1,2], L. Morawska[2], L. Stabile[1,*]

[1] Department of Civil and Mechanical Engineering, University of Cassino and Southern Lazio, Cassino, FR,

Italy

[2] International Laboratory for Air Quality and Health, Queensland University of Technology, Brisbane, Qld,

Australia

*Corresponding author:

Luca Stabile

Department of Civil and Mechanical Engineering,

University of Cassino and Southern Lazio, Cassino, FR, Italy

Via G. Di Biasio 43, 03043 Cassino (FR), Italy

e-mail: l.stabile@unicas.it

Abstract

Airborne transmission is a recognized pathway of contagion; however, it is rarely quantitatively

evaluated. This study presents a novel approach for quantitative assessment of the individual

infection risk of susceptible subjects exposed in indoor microenvironments in the presence of an

asymptomatic infected SARS-CoV-2 subject. The approach allowed the maximum risk for an

exposed healthy subject to be evaluated or, starting from an acceptable risk, the maximum

24 exposure time. We applied the proposed approach to four distinct scenarios for a prospective

25 assessment, highlighting that, in order to guarantee an acceptable individual risk of 10^{-3} for

26 exposed subjects in naturally ventilated indoor environments, the exposure time should be

27 shorter than 20 min. The proposed approach was used for retrospective assessment of

28 documented outbreaks in a restaurant in Guangzhou (China) and at a choir rehearsal in Mount

29 Vernon (USA), showing that, in both cases, the high attack rate values can be justified only

30 assuming the airborne transmission as the main route of contagion. Moreover, we shown that

31 such outbreaks are not caused by the rare presence of a superspreader, but can be likely

32 explained by the co-existence of conditions, including emission and exposure parameters, leading

33 to a highly probable event, which can be defined as a "superspreading event".

34

35 **Keywords**: SARS-CoV-2 (COVID-19) assessment; virus airborne transmission; indoor; ventilation;

36 coronavirus.

37

38 **1. Introduction**

39 The airborne transmission of a virus and the consequent contagion risk assessment is a complex

40 issue that requires multidisciplinary knowledge. It is necessary to understand the characteristics

41 and mechanisms behind the generation of respiratory microdroplets [1,2], the survival of viruses in

42 microdroplets [3], the transport of microdroplets and human exposure to them [4], and the airflow

43 patterns that carry microdroplets in buildings [5]. Expiratory human activities generate virus-

44 carrying microdroplets that are small enough to remain aloft in air during exhalation, talking, and

45 coughing [2,6,7]. Atomization occurs in the respiratory tract, and droplets are expelled at high speed

46 during expiration [8,9]. Toques of liquid originating from different areas of the upper respiratory

47 tract are drawn out from the surface and broken into droplets of different sizes [10]. The findings of

48   early investigations [11–13] served as a foundation for subsequent studies involving temporal and

49   spatial visualization methods using high-speed cameras [14], particle image velocimetry [8] and, above

50   all, increasingly accurate particle counters [6], which have facilitated the detailed characterization

51   and quantitation of droplets expelled during various forms of human respiratory exhalation flows.

52   The issue of the viral load emitted, however, remained difficult to solve. In the past, backward

53   calculation was used to estimate the emission of an infected subject based on retrospective

54   assessments of infectious outbreaks only at the end of an epidemic [15–18]. This led to the definition

55   of emission values for each virus regardless of the type of respiratory act and the metabolic

56   activity of the infected subject. Recently, the authors presented an approach to evaluate the viral

57   load emitted by infected individuals with a view to provide new predictive capacities, not currently

58   available [19]. This approach, based on the oral viral load and the infectivity of the virus, takes into

59   account the effect of other parameters such as inhalation rate, type of respiratory activity, and

60   activity level, to estimate the quanta emission rate. This value provides key information for

61   engineers and indoor air quality experts to simulate airborne dispersion of diseases in indoor

62   environments. Indeed, the use of exposure risk models in closed environments [20,21] makes it

63   possible to estimate contagion starting from the emission values of a contagious subject.

64   The overall approach of emission and exposure modelling represents an essential tool to be

65   applied in enclosed spaces, and can support air quality experts and epidemiologists in the

66   management of indoor environments during an epidemic for both prospective and retrospective

67   assessments.

68   In this paper we apply a novel approach that takes into account the characteristics of the emitting

69   subject, the microenvironment, and the exposed subject to calculate the probability of infection

70   and the individual risk, for both prospective and retrospective assessments of airborne infectious

71   transmission of SARS-CoV-2. In the case of prospective assessment, various exposure scenarios in

72   indoor environments were analyzed in order to assess the influence of risk mitigation parameters.

73   In the case of retrospective assessment, we estimated the probability of infection and the

74   individual risk of two documented outbreaks.

75   **2. Materials and methods**

76   To evaluate both prospective and retrospective assessments of the airborne transmission of SARS-

77   CoV-2, we used a four-step approach to quantify the probability of infection, i.e. the ratio between

78   infected cases and the exposed population due to exposure in a microenvironment where a SARS-

79   CoV-2 infected subject is present. The four steps of the proposed approach are: i) evaluation of

80   the quanta emission rate; ii) evaluation of the exposure to quanta concentration in the

81   microenvironment; iii) evaluation of the dose of quanta received by an exposed susceptible

82   subject; and iv) estimation of the probability of infection on the basis of a dose–response model.

83   The simulations of the probability of airborne transmission of SARS-CoV-2 were performed

84   applying a Monte Carlo method [22]. Further they adopted the infection risk assessment typically

85   implemented to evaluate the transmission dynamics of infectious diseases and to predict the risk

86   of these diseases to the public [17,20,21].

87   Once the probability of infection was obtained, an approach to evaluate the individual infection

88   risk, i.e. a parameter that also takes into account how likely the probability of infection can occur,

89   was also implemented. Individual risk can be easily compared to an acceptable risk, i.e. a target

90   reference risk that could be suggested by agencies and regulatory authorities to control the

91   pandemic. In the following sections, the methodologies adopted to evaluate the probability of

92   infection based on the four step approach (section 2.1) and the individual infection risk (section

93   2.2) are described. The application of the proposed approach for prospective and retrospective

94   assessments is described in sections 2.3 and 2.4.

95 ## 2.1 Estimation of the probability of infection

96 ### 2.1.1 Evaluation of the quanta emission rate: the forward emission approach

97 Recently, Buonanno et al. [19] proposed a forward emission approach to estimate the quanta

98 emission rate of an infectious subject on the basis of the viral load in the sputum and the

99 concentration of droplets expired during different activities. A quantum is defined as the dose of

100 airborne droplet nuclei required to infect a susceptible person. The quanta emission rate (ER_q,

101 quanta h^{-1}) was evaluated as:

102

103
$$ER_q = c_v \cdot c_i \cdot IR \cdot \int_0^{10\mu m} N_d(D) \cdot dV_d(D) \tag{1}$$

104 where c_v is the viral load in the sputum (RNA copies mL^{-1}), c_i is a conversion factor defined as the

105 ratio between one infectious quantum and the infectious dose expressed in viral RNA copies, IR is

106 the inhalation rate ($m^3 h^{-1}$), N_d is the droplet number concentration (part. cm^{-3}), and $V_d(D)$ is the

107 volume of a single droplet (mL) as a function of the droplet diameter (D). The number and volume

108 of the droplets (V_d) is determined on the basis of data obtained experimentally by Morawska et al.

109 (2009)[6].

110 With reference to the SARS-CoV-2 viral load in the mouth, researchers have recently found c_v

111 values of up to 10^{11} copies mL^{-1}, which is also variable in the same patient during the course of the

112 disease [23–26]. In particular, Rothe et al. [24] reported a case of SARS-CoV-2 infection in which

113 transmission appears to have occurred during the incubation period in the index patient. A high

114 viral load of 10^8 copies mL^{-1} was found, confirming that asymptomatic persons are potential

115 sources of SARS-CoV-2 infection. Furthermore, Pan et al. [23], in a study on 82 SARS-CoV-2 infected

116 patients, found c_v values in the range of $10^8–10^9$ RNA copies mL^{-1}, also in the previous days and in

117 the first days of onset of the disease. Consequently, the concentrations of the viral load in the

118 mouth can reach values of 10^9 RNA copies mL^{-1} and occasionally up to 10^{11} RNA copies mL^{-1} during

119 the course of the disease.

120 The conversion factor, c_i, i.e. the ratio between one infectious quantum and the infectious dose

121 expressed in viral RNA copies, barely represents the probability of a pathogen surviving inside the

122 host to initiate the infection; thus $c_i=1$ implicitly assumes that infection will occur for each

123 pathogen (RNA copy in the case of SARS-CoV-2) received by the exposed people. There are

124 currently no values available in the scientific literature for c_i for SARS-CoV-2. Watanabe et al. [27]

125 estimated the infectious doses of several coronaviruses on the basis of data sets challenging

126 humans with virus HCoV-229E (known as an agent of human common cold) and animals with

127 other viruses (e.g. mice with MHV-1, considered as a surrogate of SARS-CoV-1). On the basis of the

128 orders of magnitude of the infectivity conversion factors for the overall data sets, we assumed a c_i

129 range between 0.01 and 0.1.

130 The quanta emission rate calculation was performed for four different emission profiles (which are

131 adopted in the risk evaluations described later) evaluated as a combination of expiratory activities

132 and activity levels: (i) oral breathing during resting; (ii) oral breathing during heavy activity; (ii)

133 speaking during light activity; and (iv) singing (or loudly speaking) during light activity.

134 Quanta emission rates were calculated using eq. (1) and applying a Monte Carlo method [22] in order

135 to take into account for the possible variation of the input data. To this end, probability density

136 functions characteristics of each parameter were considered. In particular, we considered normal

137 distributions for: (i) the log-transformed c_v data (average and standard deviation of $\log_{10}(c_v)$ equal

138 to 8 and 0.7 $\log_{10}$ (RNA copies mL^{-1}), respectively); and (ii) the infectious dose c_i (average and

139 standard deviation equal to 0.025 and 0.125, respectively). A distribution of quanta emission rates

140 (ER_q), was obtained as a result of application of the Monte Carlo method (Figure 1), i.e. the

141 probability density function of ER_q (pdf_q).

142   *2.1.2   Evaluation of the exposure to quanta concentration*

143   The second step in evaluating the probability of infection is evaluation of the quanta

144   concentration to which a susceptible subject is exposed. The quanta concentration at time t, $n(t)$,

145   in an indoor environment is based on the quanta mass balance proposed by Gammaitoni and

146   Nucci [20], and can be evaluated as:

147

148    $$n(t) = \frac{ER_q \cdot I}{IVRR \cdot V} + \left(n_0 - \frac{ER_q \cdot I}{IVRR}\right) \cdot \frac{e^{-IVRR \cdot t}}{V} \qquad \text{(quanta m}^{-3}\text{)} \qquad (2)$$

149   where $IVRR$ (h^{-1}) represents the infectious virus removal rate in the space investigated, n_0

150   represents the initial number of quanta in the space, I is the number of infectious subjects, V is the

151   volume of the indoor environment considered, and ER_q is the quanta emission rate (quanta h^{-1}) for

152   the specific disease/virus under investigation. The quanta concentration calculation adopted here

153   is based on the following hypotheses: the quanta emission rate is considered to be constant, the

154   latent period of the disease is longer than the time scale of the model, and the droplets are

155   instantaneously and evenly distributed in the room [20]. The infectious virus removal rate is the sum

156   of three contributions [28]: the air exchange rate (AER) via ventilation, the particle deposition on

157   surfaces (k, e.g. via gravitational settling), and the viral inactivation (λ). The deposition rate was

158   evaluated as the ratio between the settling velocity of super-micrometric particles [roughly

159   1.0×10^{-4} m s^{-1} as measured by Chatoutsidou and Lazaridis [29]] and the height of the emission

160   source (1.5 m); thus, k was 0.24 h^{-1}. The viral inactivation was evaluated on the basis of the SARS-

161   CoV-2 half-life (1.1 h) detected by van Doremalen et al.[3], thus λ was 0.63 h^{-1}.

162   In the exposure scenarios tested with the prospective and retrospective approaches, to take the

163   variability of the input parameters into account, the indoor quanta concentration n(t) was

164   determined through eq. (2), applying a Monte Carlo method that adopted the probability density

165   functions (pdf$_q$) characteristic of quanta emission rates (ER$_q$). Since the probability density

166   functions of the log-transformed $\log_{10}(ER_q)$ for the different expiratory activities resulted in a

167   normal distribution (Shapiro-Wilk test, $p < 0.01$), the quanta concentration $n(t)$ was evaluated by

168   providing a Gaussian distribution of $\log_{10}(ER_q)$ (average and standard deviation values are is

169   summarized in the results section; see Table 2) and then applying a back-transformation from

170    $\log_{10}(ER_q)$ to ER_q. The relative frequency at which a certain quanta concentration occurred for each

171   time step of simulation, i.e. the probability density function of the quanta concentration (pdf_n),

172   was also obtained as result of the Monte Carlo simulations.

173   *2.1.3   Evaluation of the dose of quanta received by an exposed susceptible subject*

174   The dose of quanta received by a susceptible subject exposed to a certain quanta concentration,

175    $n(t)$, for a certain time interval, T, can be evaluated by integrating the quanta concentration over

176   time as:

177

178
$$D_q = IR \int_0^T n(t)dt \qquad \text{(quanta)} \qquad (3)$$

179   It can be concluded from Eq. (3) that the dose of quanta received by a susceptible subject is

180   affected by the inhalation rate (IR) and subsequently by their activity level. As an example, for the

181   same exposure scenario [i.e. identical $n(t)$ and T], the dose of quanta received by subjects

182   performing at a light activity level (IR = 1.38 m^3 h^{-1}; e.g. slowly walking) is more than double that

183   received by people just sitting or standing (IR = 0.54 m^3 h^{-1}). For the dose, in the exposure

184   scenarios described in this paper, the Monte Carlo method was applied to eq. (3) considering the

185   probability density function of the quanta concentration (pdf_n), whereas the IR was considered as

186   a constant value; thus, the probability density function of the dose (pdf_D) was obtained for each

187   time step of the simulation.

188 *2.1.4   Evaluation of the probability of infection through a dose–response model*

189 The fourth and final step in evaluating the probability of infection is the adoption of a dose–

190 response model. Several dose–response models are available in the scientific literature for

191 assessing the probability of infection of airborne-transmissible pathogens [16,17], including

192 deterministic and stochastic models, and threshold and non-threshold models.

193 The best-suited dose–response models for airborne transmission of pathogens are the stochastic

194 models. In particular, exponential models have been mostly adopted in previous studies because

195 of their suitability and simplicity [27]. Such models consider the pathogens as discrete bundles (i.e.

196 quanta) distributed in a medium (e.g. saliva/sputum) in a random manner described by the

197 Poisson probability distribution. When the medium is aerosolized, the pathogen distribution in the

198 aerosols, and hence their distribution in the air, also follows the Poisson probability distribution.

199 The complex Poisson summation equations can be simplified in an exponential equation [17,27,30], i.e.

200 the exponential dose–response model, which evaluates the probability of infection, P_I (%), of

201 susceptible people as:

202

203 $$P_I = 1 - e^{-D_q} = \frac{c}{S} \qquad (\%) \qquad\qquad (4)$$

204 For a unit dose of quanta ($D_q = 1$), the probability of infection P_I is equal to 63%, from which

205 derives the definition of "quantum" as the "amount of infectious material to infect 1-e^{-1} (i.e. 63%)

206 of the people in an enclosed space" [13,20].

207 In the exponential dose–response model, the variation of host sensitivity to the pathogen is not

208 considered. More complex models, such as the Beta-Poisson probability distribution, could take

209 this factor into account [17,27,30]; nonetheless, in the present paper the differences in the exposed

210 population in terms of susceptibility to the virus will not be considered.

211   The probability of infection P_I evaluated in the following exposure scenarios was determined

212   through eq. (4), also applying a Monte Carlo method. To this end, the probability density functions

213   of the dose of quanta (pdf_D) obtained as a result of the Monte Carlo simulation on D_q were

214   considered; thus, a probability density function of P_I was also obtained (pdf_P).

215   The probability of infection represents the ratio between the number of infection cases (C) and

216   the number of exposed susceptibles (S). In retrospective analyses of documented outbreaks, the

217   known C/S ratio is typically defined as the "attack rate".

218   *2.2   The individual infection risk and the basic reproduction number*

219   As stated above, the probability of infection (P_I) is the expected number of infection cases in

220   relation to the number of exposed susceptibles (C/S ratio). However, based on eqs. (2-4), such

221   probability is strongly influenced by the probability density function of the dose (pdf_D), which is

222   influenced in turn by the probability density function of the quanta concentration (pdf_n) and by

223   the probability density function of the quanta emission rate (pdf_q). In other words, for a given

224   exposure scenario (microenvironment, ventilation, inhalation rate of the exposed subject, etc.) the

225   probability of infection (P_I) can assume different values on the basis of the rate of quanta emitted

226   by the infected subject: the lower the quanta emission rates, the lower the probability of infection

227   (since all the other parameters affecting the exposure were considered to be constant values).

228   Thus, when evaluating the individual risk (R) of an exposed person, we should know both the

229   probability of infection (P_I) and the probability of occurrence of such a P_I value (P_P). The latter is

230   defined by the probability density function pdf_P. Since the probability of infection (P_I) and the

231   probability of occurrence P_P are independent events, the individual infection risk, R, can be

232   evaluated as the product of the two terms:

233

234                               $$R = P_I \cdot P_P \qquad\qquad (\%) \qquad\qquad (5)$$

235

236   The probability density function of the individual risk, pdf_R, can be obtained by multiplying all the

237   possible P_I values obtained from the application of the Monte Carlo method to the four-step

238   approach by the corresponding probability of occurrence. The maximum value of R in eq. (5), i.e.

239   the mode of the pdf_R, is of particular interest because it represents the most probable individual

240   risk for a healthy subject or, in other words, the highest probability of being infected. In a

241   conservative application of the proposed approach to estimate and reduce the risk of individuals

242   being together with an infected individual in an indoor environment, the maximum individual

243   infection risk must be less than an acceptable risk.

244   The US Environmental Protection Agency (EPA) typically uses a target reference risk range of 10^{-4}

245   to 10^{-6} for carcinogens in drinking water [31], which is in line with World Health Organization (WHO)

246   guidelines for drinking water quality, which base guideline values for genotoxic carcinogens on the

247   upper bound estimate of an excess lifetime cancer risk of 10^{-5} [32]. If the estimated lifetime cancer

248   risk is lower than 10^{-6}, the risk is considered acceptable, while risks above 10^{-4} are considered

249   unacceptable [33].

250   The choice of an acceptable contagion risk for SARS-CoV-2 is difficult and certainly questionable.

251   However, considering the mortality rate of SARS-CoV-2, this turns out to be an order of magnitude

252   lower than the corresponding value associated with carcinogenic diseases. For this reason, only for

253   discussion purposes, the value of 10^{-3} is taken as an acceptable risk reference for SARS-CoV-2.

254   For the purpose of managing an epidemic and keeping the infection under control, it is also

255   important to estimate the basic reproduction number of the infection, R_0, which is calculated as

256   the ratio between the number of susceptible people infected (C) and the infected subject (I). Thus,

257   R_0 can be easily evaluated by multiplying the infection probability, P_I, by the number of exposed

258   susceptible individuals (S). To control an epidemic, the R_0 value must be less than 1. Therefore, in

259   addition to estimating an acceptable individual infection risk, it is necessary to specifically verify

260   that, with the crowding expected within the environment, the corresponding value of R_0 is less

261   than 1.

262   *2.3   Scenarios in the prospective assessment*

263   The proposed four-step approach was applied to different indoor microenvironments by varying

264   the main parameters in order to evaluate the effect of the influencing parameters. In particular,

265   four emission profiles of the infected subject [6] and corresponding profiles of the healthy subjects

266   exposed were chosen. For the sake of simplicity, the simulations were run assuming that the

267   susceptible subjects remained in the microenvironment for the same length of time as the

268   infected subject (i.e. the two subjects enter and leave the environment under test together). Each

269   indoor environment under investigation was tested for three different values of air exchange rate

270   (AER). Table 1 presents a detailed summary of the four different indoor exposure scenarios

271   considered to evaluate the risk of airborne transmission of SARS-CoV-2. Scenario A consists of a

272   hospital room of 100 m^3 where a resting infected patient emits quanta in the room through oral

273   breathing, whereas the exposed susceptible subjects consist of a member of the medical staff in a

274   light exercise activity (scenario A-1) and another patient at rest (scenario A-2). In scenario B, the

275   infection affects two subjects, both oral breathing during a sports activity in a 300 m^3 gym.

276   Scenario C concerns two subjects (infected and healthy) in light activity while speaking in a generic

277   300 m^3 office (bank, post office, supermarket, shop, etc.). Finally, scenario D represents an

278   infected subject singing or speaking loudly in an 800 m^3 room with healthy subjects listening at a

279   sedentary activity level.

280   **Table 1** - Description of the exposure scenarios tested in the prospective assessment.

	Scenario A	Scenario B	Scenario C	Scenario D

Type of indoor environment	Hospital room	Gym	Public indoor environments (e.g. restaurant, bank)	Conference room or auditorium
Emitting subject	Patient (Resting, oral breathing)	Exercising person (heavy exercise, oral breathing)	Speaking person (light exercise, voiced counting)	Singer or conference loud speaker (light exercise, unmodulated vocalization)
Exposed subject	A-1. Medical staff (light exercise) A-2. Patient (resting)	Exercising person (heavy exercise)	Speaking person (light exercise)	Spectator (sedentary activity)
Volume (m^3)	100	300	300	800
Ventilation, AER (h^{-1})	• Natural ventilation 0.5 h^{-1}, • Mechanical ventilation 3 h^{-1}, • Mechanical ventilation 10 h^{-1}			
Deposition rate, k (h^{-1})	0.24			
Inactivation rate, λ (h^{-1})	0.63			

281 *2.4 Retrospective assessments: outbreaks in a restaurant in Guangzhou, China, and at choir*

282 *rehearsal in Skagit Valley (USA)*

283 *2.4.1 The outbreak in a restaurant in Guangzhou, China*

284 A possible case of airborne transmission was recently documented by Lu et al.[34]. Here, an index

285 case patient traveled from the Chinese epidemic epicenter, Wuhan, on 23 January 2020 and ate

286 lunch in a restaurant in Guangzhou, China, with his family on 24 January 2020 (family A, 10 people

287 sitting at the same table). Later that day, the index patient experienced onset of fever and cough

288 and SARS-CoV-2 infection was diagnosed. On the following days, nine other people were

289 diagnosed with SARS-CoV-2 infection: four members from family A's table and five other people at

290 two different tables (families B and C). No other customers seated at other tables or waiters were

291 infected.

292 The restaurant is a 5-floor building without windows; each floor has its own air ventilation system.

293 The third floor dining area, at which the index patient ate lunch, has a floor area of 145 m^2, with

294 15 tables arranged with a distance between each table of about 1 m. A total of 91 people (83

295 customers, 8 staff members) were in the room during that lunch. The exposure time was variable

296 for the customers: those seated at tables close to the index patient had exposure times of

297 53 minutes (family B) and 73 minutes (family C). The ventilation and air conditioning situation is

298 reported in Lu et al.[34]. Five fan coil air-conditioning units are installed in the room and there is no

299 outdoor air supply; thus, the ventilation relies only upon infiltration and natural ventilation. The

300 authors performed computational fluid dynamics analyses and tracer gas decay tests to obtain

301 more information about the possible air-flow pathway in the room, and to determine the air

302 exchange rate expected during that lunch. The analyses performed showed that, due to the

303 particular installation and use of the fan coils, the room can be divided into different air-flow

304 zones, with well-mixed conditions. The air-flow zone involving the table at which the index patient

305 sat also included the two tables at which the other five infected people sat; and covered an area

306 of roughly 45 m^3. The tracer gas decay tests revealed a low air exchange rate (mostly due to the

307 absence of an outdoor air supply) in the range of 0.56–0.77 h^{-1}.

308 Therefore, on the basis of the available information, the retrospective assessment was applied to

309 this outbreak case, through eqs. (2) and (3), using the following input data: i) room volume of

310 45 m^3; ii) documented probability of infection, i.e. attack rate, of 45% (i.e. 5 out of 11 people of

311 families B and C (family A members were excluded as they could easily have been infected through

312 other infection routes); iii) average exposure time of 1 h; iv) speaking at a light activity level for all

313 people (both emitting and exposed subjects), and v) average AER = 0.67 h^{-1}.

314 *2.4.2 The outbreak at a choir rehearsal in Skagit (USA)*

315 A further possible case of airborne transmission of SARS-CoV-2 was documented by the USA

316 media (www.latimes.com/world-nation/story/2020-03-29/coronavirus-choir-outbreak). This case

317 was recorded on 10 March, in Mount Vernon (Skagit County, Washington State, USA). In a 810 m^3

318 hall, 61 choir members (out of a total of 121 regular members) gathered to rehearse, aware of the

319 practices for the containment of contagion (frequent hand washing and social distancing). None of

320 the members that attended had evident symptoms of SARS-CoV-2 infection. There was hand

321 sanitizer at the front door and members refrained from the usual hugs and handshakes; each

322 person brought their own sheet music. The event lasted from 6:30 pm to 9:00 pm (about 2.5

323 hours). Within few days, 33 of the 61 participants (53%) were diagnosed with SARS-CoV-2

324 infection, at least three were hospitalized, and two died [35].

325 As pointed out by Hamner et al.[35], the 2.5-hour singing practice could have provided several

326 opportunities for droplet and fomite transmission (e.g. members sitting close to one another,

327 sharing snacks, and stacking chairs at the end of the practice). Nonetheless, the abovementioned

328 voluntary measures put in place would not support the documented spread of the contagion. On

329 the contrary, the act of singing, itself, might have contributed to transmission through emission of

330 aerosols, which is affected by loudness of vocalization [19]. This is even more relevant considering

331 that attack rate of 53.3% (based on 33 confirmed cases) could represent a conservative estimate,

332 since other 20 probable cases were mentioned by Hamner et al.[35].

333 As regard the heating and ventilating system, limited information is available: the Fellowship Hall

334 is heated by a relatively new commercial forced-air furnace with supply and return air grills

335 situated high on a single wall. The furnace is installed to have both make-up and combustion air,

336 but it is not known how much fresh air was provided on that evening. During the entire rehearsal

337 no exterior doors were open. We applied a retrospective assessment to the case of the Skagit

338   Valley choir through eqs. (2) and (3), using the following input data: i) room volume of 810 m³; ii)

339   documented probability of infection, i.e. attack rate, equal to 53%; iii) exposure time of 2.5 h; iv)

340   singing at a light activity level for all people; and v) natural ventilation with an AER = 0.5 h^{-1}.

341   **3. Results and Discussions**

342   *3.1   Statistics of quanta emission rates*

343   Figure 1 and Table 2 show the statistics relating to the quanta emission rates for the four emission

344   profiles considered in section 2.1. As shown in Buonanno et al.[19], there are large differences

345   between the emission profiles. Obviously the lowest values are found under the oral breathing

346   condition during resting (median value of 0.36 quanta h^{-1}), followed by the oral breathing

347   condition during heavy activity as the inhalation rate increases (2.4 quanta h^{-1}), and reaching 4.9

348   quanta h^{-1} for the increase in aerosol emitted during vocalization [6] and, finally, peaking during

349   singing/speaking loudly (31 quanta h^{-1}). Indeed, the rate of particle emission during normal human

350   speech is positively correlated with the amplitude of vocalization [36].

351   The probability density functions of the quanta emission rates (P_q) were also determined. In

352   particular, the log-transformed ER_q values obtained from the Monte Carlo simulations resulted in a

353   normal distribution (Shapiro-Wilk test, $p < 0.01$). Table 2 shows the average and standard

354   deviation values of the $\log_{10}(ER_q)$.

355   We point out that the estimated values present two main uncertainty contributions clearly related

356   to the limited data currently available for the SARS-CoV-2: i) a still low number of experimental

357   data for the viral load in the mouth, c_v, of SARS-CoV-2 infected subjects, ii) unavailable infectivity

358   conversion factors, c_i, for SARS-CoV-2; indeed, as mentioned in the methodology section, the c_i

359   parameter was estimated on the basis of data available for other coronaviruses challenging

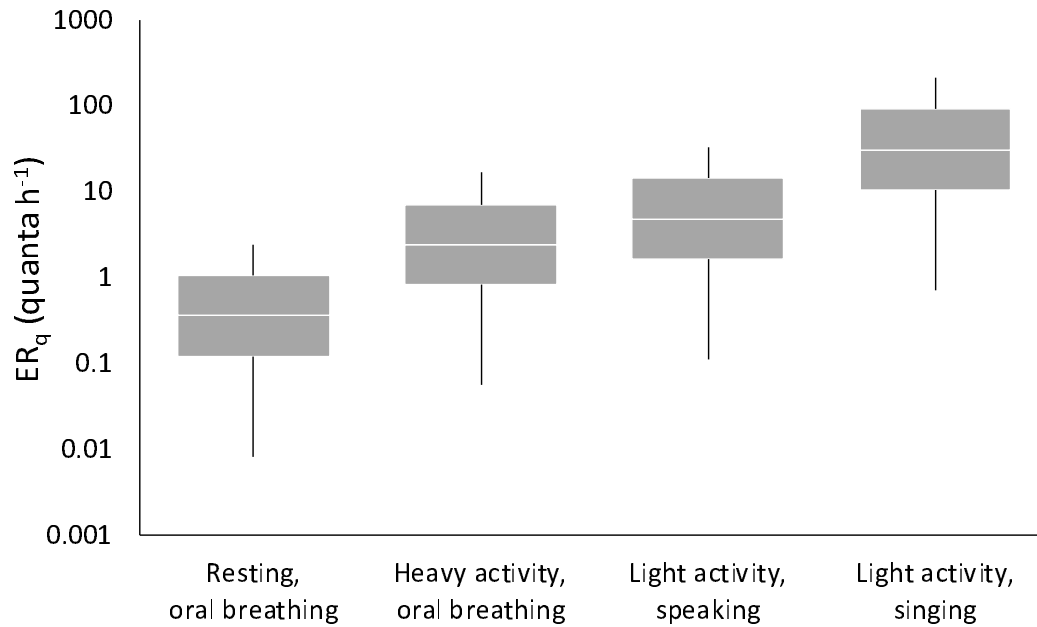360   humans (only in the case of HCoV-229E) and animals (for all other types of coronavirus).

361

Figure 1 - Statistics of quanta emission rates (ER_q) for the four expiratory activities considered in the

exposure scenarios. Data reported represent 1st, 25th, 50th, 75th, and 99th percentiles.

Table 2 - ER_q (quanta h^{-1}) and log(ER_q) statistics for SARS-CoV-2 as a function of the expiratory activity and

activity level. The log-transformed ER_q values follow a log-normal distribution; thus, the average and

standard deviation values of the $\log_{10}(ER_q)$ are provided.

		Resting, oral breathing	Heavy activity, oral breathing	Light activity, speaking	Light activity, singing (or speaking loudly)
ER_q	5th percentile	2.5×10^{-2}	1.7×10^{-1}	3.4×10^{-1}	2.1×10^{0}
	25th percentile	1.2×10^{-1}	8.1×10^{-1}	1.6×10^{0}	1.0×10^{1}
	50th percentile	3.6×10^{-1}	2.4×10^{0}	4.9×10^{0}	3.1×10^{1}
	75th percentile	1.1×10^{0}	7.2×10^{0}	1.5×10^{1}	9.3×10^{1}
	95th percentile	5.2×10^{0}	3.0×10^{1}	7.1×10^{1}	4.5×10^{2}
	99th percentile	1.6×10^{1}	1.1×10^{2}	2.2×10^{2}	1.4×10^{3}
$\log_{10}(ER_q)$	Average	-4.4×10^{-1}	3.9×10^{-1}	6.9×10^{-1}	1.5×10^{0}
	Stand. dev	7.1×10^{-1}	7.1×10^{-1}	7.1×10^{-1}	7.1×10^{-1}

367   *3.2*   *Risk management in prospective assessment applications*

368   *3.2.1   Illustrative example of probability of infection and individual risk evaluation*

369   In Figure 2 an illustrative example of quanta concentration $n(t)$, dose of quanta (D_q), and

370   probability of infection (P_I) trends as a function of time (here shown for 2 h) resulting from the

371   Monte Carlo simulation for exposure scenario D (singing exhibition, conference speaker) with an

372   AER = 0.5 h^{-1} is shown. In particular, the trends of different percentiles are reported. The example

373   shows that a person singing/speaking loudly in such a microenvironment can lead to a median $n(t)$

374   value after 2 hours equal to 0.027 quanta h^{-1} (with a 5th–95th percentile range of < 0.002–

375   0.38 quanta h^{-1}). Such concentrations lead to a median dose of quanta received by the subject

376   exposed for 2 h in a sedentary activity equal to 0.029 quanta (with a 5th–95th percentile range of

377   < 0.002–0.42 quanta), then resulting in a median probability of infection, P_I, of 2.8% (with a 5th–

378   95th percentile range of 0.2%–33.0%). Thus, if higher quanta emission rates are considered, the

379   indoor quanta concentrations and the consequent probability of infection can be more than 10-

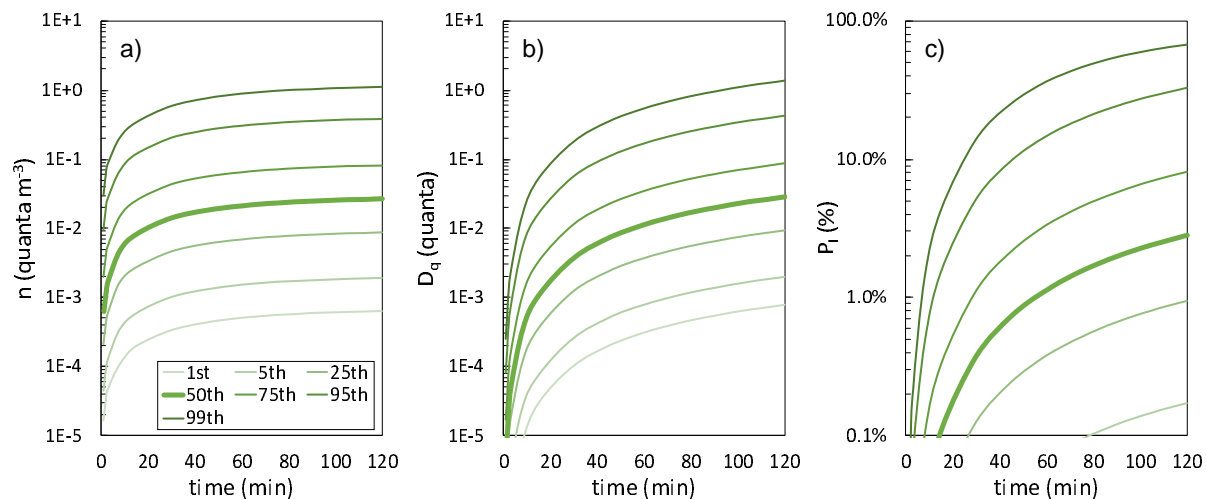380   fold the median values.

381

382

383   **Figure 2** - Trends of quanta concentration (a), dose of quanta (b), and probability of infection (c) as a

384   function of time (here shown for 2 h of exposure) resulting from the Monte Carlo simulation for exposure

385   scenario D with an AER = 0.5 h^{-1}. Different percentiles are reported.

386   In view of the application of a conservative approach that could be essential to reduce the risk of

387   contagion in indoor environments, using the highest quanta concentration and probability of

388   infection values can be misguiding. Indeed, the probability of occurrence of such high values is

389   extremely low. Thus, as described in section 2.2, a proper evaluation of the individual infection risk

390   (R) can be obtained by applying eq. (4), i.e. multiplying the probability of infection (P_I) by the

391   corresponding probability of occurrence (P_P). In Figure **3** the probability density functions of

392   individual infection risk (pdf_R), probability of infection (pdf_P), quanta concentration (pdf_n), and

393   dose of quanta (pdf_D) after 2 hours of exposure are reported (in terms of R, P_I, n and D_q values for

394   each percentile) for the illustrative example discussed above (i.e. scenario D, AER = 0.5 h^{-1}). The

395   individual infection risk (R) presents a maximum value (R_{max}) at the 85th percentile (2.2%) due to a

396   probability of infection P_I = 14.5% and a probability of occurrence P_P = 15%. In other words, the R

397   value at the 85th percentile is the most probable individual infection risk for a healthy susceptible

398   subject (i.e., the one with the highest chance of occurring). Due to the similarity of the probability

399   density functions of the four expiration activities resulting from the calculation of the quanta

400   emission rates ($log_{10}(ER_q)$ reported in Table 2), the pdf_R for all the exposure scenarios tested here

401   was similar to that of the exposure scenario shown in Figure 3 (i.e. the R_{max} value occurs in the

402   narrow range of 84th–90th percentile).

403   Furthermore, as discussed in section 2.2, the probability density function of the probability of

404   infection (pdf_P) is mostly influenced by the probability density function of the quanta emission rate

405   (pdf_q) when moving backwards in the four-step approach; indeed, once the exposure scenario is

406   defined, all the parameters contributing to the calculation of P_I (ventilation, room volume, subject

407   activity, etc.) can be considered as constant values. Thus, for a simplified estimate of R_{max}, the

408   simplest calculation can be applied (instead of the Monte Carlo method) by just adopting the 85th

409   percentile of the quanta emission rate in the four-step calculation using eqs. (2-4).
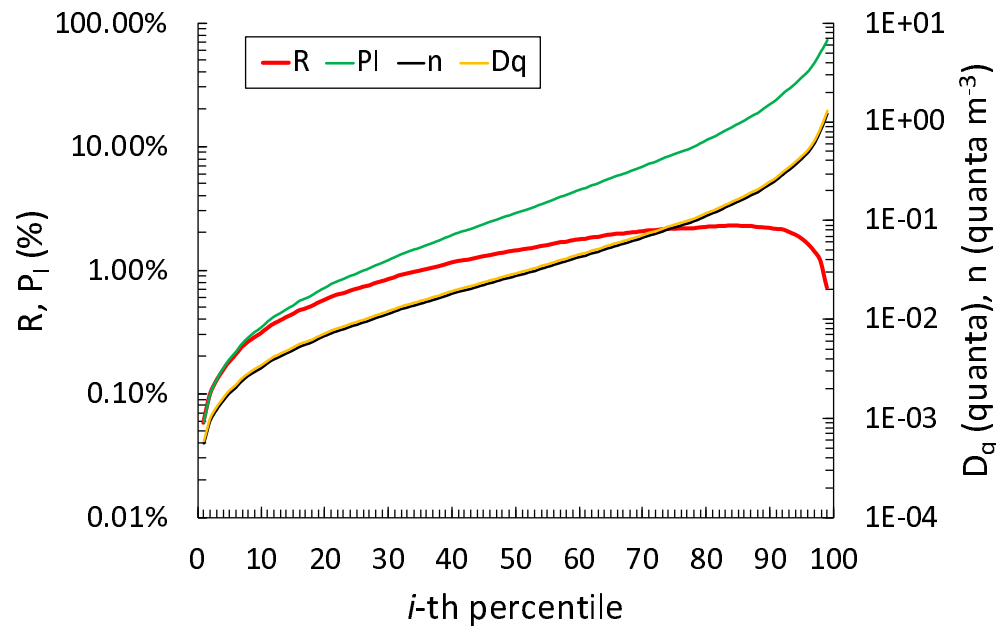

410

411   **Figure 3** – Probability density functions of individual infection risk, probability of infection, quanta

412   concentration, and dose of quanta at t = 120 min for the illustrative example reported in Figure **2** (exposure

413   scenario A with an air exchange rate of 0.5 h^{-1}). The probability density functions are reported as quanta

414   concentration (n), dose of quanta (D_q), probability of infection (P_I), and individual infection risk (R) for each

415   percentile. The maximum individual infection risk (R_{max}) is 1.9% and occurs at the 85th percentile

416   (P_I = 14.5%, P_q = 15%).

417   *3.2.2   Estimate of the maximum individual risk versus exposure time in indoor environments*

418   Figure 4 and Table 3 show the results of the Monte Carlo simulations for the four exposure

419   scenarios analyzed. The exposure time–risk relationships reported in Figure 4 are essential as they

420   can be used by choosing either the exposure time or the maximum risk R_{max} as the independent

421   variable. In the first case, knowing the exposure time of the healthy subject in the environment in

422   question, the corresponding individual infection risk can be evaluated and then compared to an

423   acceptable infection risk. In the second case, once an acceptable infection risk has been imposed,

424   the corresponding maximum exposure time value can be easily assessed. The four scenarios are

425   examined assuming an acceptable risk value of 10^{-3} as discussed in section 2.3. Since the maximum

426   value of individual risk occurs roughly at the 90th percentile, the corresponding probability of

427   occurrence of the risk (P_P) is 10%; thus, an acceptable individual infection risk of 10^{-3} will roughly

428   correspond to a probability of infection of P_I = 1%. For indoor environments characterized by high

429   crowding indexes a P_I < 1% is essential as it can assure a R_0 < 1 when crowded with up to 100

430   people. Therefore, assuring an individual infection risk of 10^{-3} also guarantees the control of the

431   epidemic with an R_0 < 1 for a maximum number of exposed healthy people S < 100.

432   For the exposure scenario discussed above (scenario D, AER = 0.5 h^{-1}) the maximum exposure time

433   to reach an accepted risk of R = 10^{-3} is very short (16 min); this is due to the high viral load emitted

434   during singing or speaking loudly leading to high quanta concentrations despite the large volume

435   available. Obviously, the exposure time can increase with higher ventilation rates, e.g. reaching

436   38 min in the case of mechanical ventilation at 10 h^{-1}. The crowding index of such an indoor

437   environment (800 m^3) ranges from 0.75 m^2 (auditorium) to 2 m^2 (conference room) per person [37];

438   thus, for a room height of 4 m a corresponding floor area of 200 m^2 will be available, then

439   resulting in a total number of people simultaneously present in the room (S) ranging from 100

440   (conference room) to 267 (auditorium). Therefore, after 16 min of exposure in the case of natural

441   ventilation (or 38 min in the case of mechanical ventilation with AER = 10 h^{-1}), the value of R_0 will

442   be higher (auditorium) or equal (conference room) to 1. Thus, in the management of the

443   epidemic, reducing the crowding index could be essential. Accepting higher R_{max} values would

444   clearly increase the maximum exposure time; indeed, in the case of R_{max} = 10^{-2}, the exposure time

445   values would be 62 min and 392 min, for an AER equal to 0.5 h^{-1} and 10 h^{-1}, respectively. However,

446   in this case, the corresponding value of R_0 would be lower than 1 only for a number of exposed

447   subjects lower than 10.

448   In scenario C, the infected subject in light activity speaks in a 300 m^3 environment, along with the

449   healthy subject. The simultaneous reduction of both the quanta emission rate and the volume

450   compared to scenario D makes the maximum exposure times for an acceptable infection risk of 10^-

451   ^{3} comparable to the previous case (15 min and 36 min for ventilation of 0.5 h^{-1} and 10 h^{-1},

452   respectively). Additionally, in this case, the estimated exposure times would guarantee an $R_0 < 1$
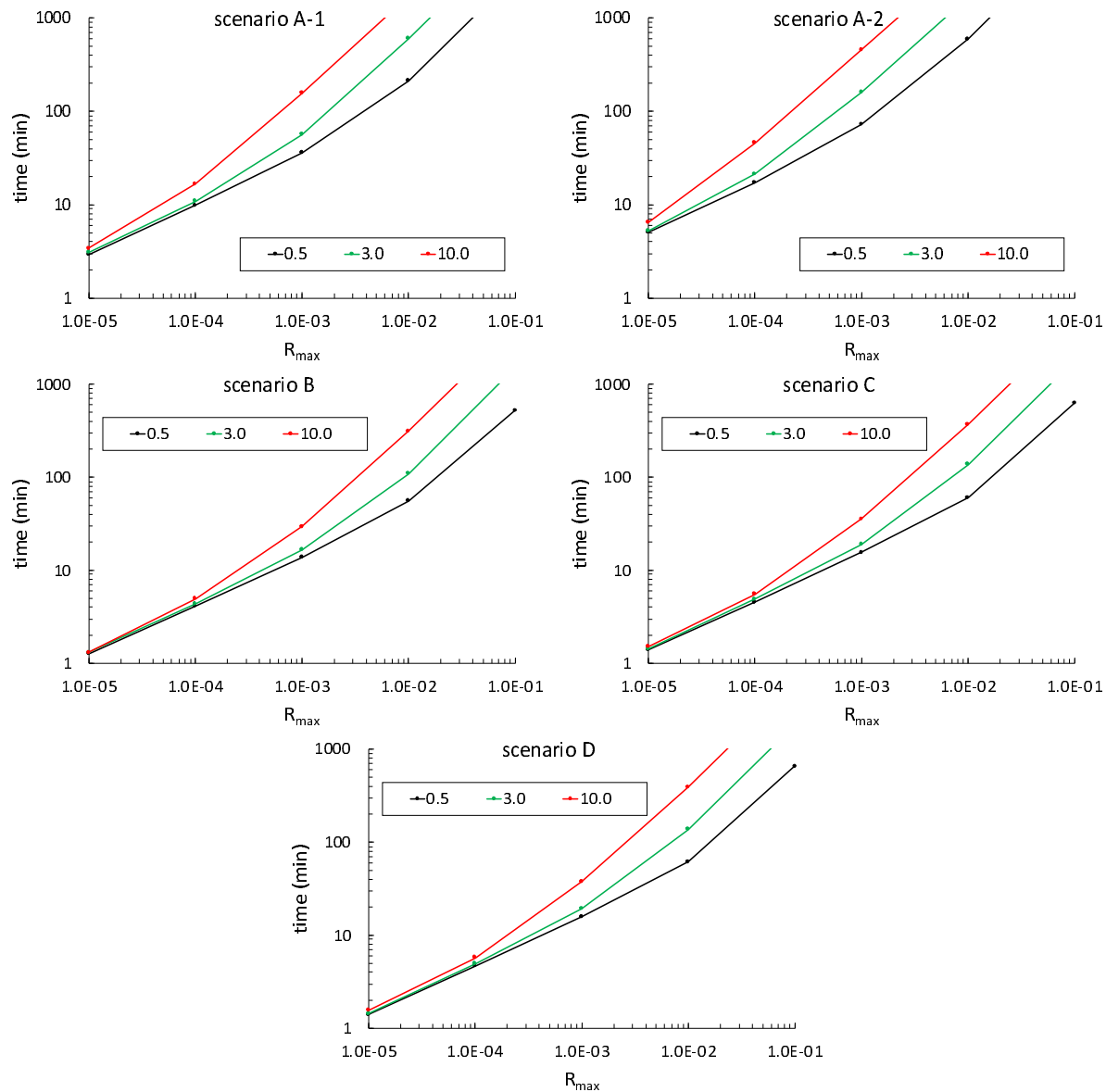
453   with S < 100 subjects.

454

Figure 4 – Relationship between time of exposure and individual risk (R) as a function of the air exchange rate (0.5 h^{-1}, 3 h^{-1}, and 10 h^{-1}) for the exposure scenarios investigated in the prospective approach and summarized in Table 1.

In scenario A (patient emitting at rest in oral breathing), the maximum exposure time in a hospital room of 100 m^3 for both a medical staff member (scenario A-1) and a patient at rest without infection (scenario A-2) is evaluated. In both cases the exposure times increase significantly with the ventilation rate, reaching 36 min and 157 min (scenario A-1), and 72 min and 455 min (scenario A-2) with AER values of 0.5 h^{-1} and 10 h^{-1}, respectively. However, despite the small size

464   of the room, the ER_q was extremely small (Table 2); thus, unless a large number of infected

465   subjects is simultaneously present in the room, the concentration of viral load in a hospital room

466   can be considered low; nonetheless, the overall risk may become relevant due to the long

467   exposure times (of 36 and 157 min). Finally, in exposure scenario B (the gym with infected and

468   healthy subjects during heavy activity with oral breathing), although there is no vocalization in the

469   subject's activity, the high inhalation rate produces considerable ER_q values, then increasing the

470   individual risk; thus, in order to guarantee an acceptable infection risk of 10^{-3} the maximum

471   exposure times resulted quite short, i.e. 14 min and 29 min for 0.5 h^{-1} and 10 h^{-1}, respectively.

472   Thus, for all the scenarios investigated, the ventilation conditions strongly influence the risk (or

473   the exposure time) of the exposed subject: this difference increases as the accepted risk increases

474   as shown in the trends presented in Figure 4. In contrast, if a lower risk was accepted (i.e. 10^{-4} or

475   10^{-5}), increasing the air exchange rate is not leading to the significant reduction of the risk, and

476   local exhaust ventilation would be more effective.

477   **Table 3** – Maximum exposure time (min) for the different exposure scenarios to reach an acceptable

478   maximum individual infection risk (R_{max}).

Exposure scenarios	AER (h^{-1})	Maximum individual infection risk (R_{max})				
		1×10^{-1}	1×10^{-2}	1×10^{-3}	1×10^{-4}	1×10^{-5}
Scenario A-1 - Hospital room	0.5	2797	212	36	10	3
Emitting subject: patient	3.0	7968	600	56	11	3
Exposed subject: Medical staff	10.0	22430	1727	157	17	3
Scenario A-2 - Hospital room	0.5	8039	597	72	17	5
Emitting subject: patient	3.0	21739	1678	159	21	5
Exposed subject: patient	10.0	64333	4671	455	46	6
Scenario B – Gym	0.5	519	55	14	4	1
Emitting subject: Exercising person	3.0	1500	110	16	4	1

Exposed subject: Exercising person	10.0	4119	314	29	5	1
Scenario C – Public indoors	0.5	627	60	15	5	1
Emitting subject: Speaking person	3.0	1812	137	19	5	1
Exposed subject: Speaking person	10.0	4807	372	36	6	1
Scenario D – Conference room	0.5	652	62	16	5	1
Emitting subject: Singer	3.0	1826	138	19	5	1
Exposed subject: Spectator	10.0	5187	392	38	6	2

479 *3.3 Retrospective assessment application: the outbreaks in a restaurant in Guangzhou and at a*

480 *choir rehearsal in Skagit Valley*

481 Figure 5 shows the trends of quanta concentration and probability of infection (P_I) evaluated for

482 the retrospective cases defined in section 2.4 (a restaurant in Guangzhou and the Skagit Valley

483 choir). The retrospective analysis applied to the restaurant in Guangzhou (Figure 5a) revealed that,

484 under the boundary conditions considered in the simulation (in terms of room volume, ventilation,

485 number of exposed people; see section 2.4.1), a probability of infection (P_I) after 1 hour of

486 exposure equal to the attack rate (45%) can be reached for a quanta emission rate of

487 $ER_q = 61$ quanta h^{-1}. This emission rate, for an emitting subject speaking during light exercise,

488 occurs at the 93rd percentile of the probability density function of ER_q (P_q).

489 Similarly, for the retrospective analysis applied to the Skagit Valley choir (Figure 5b), in order to

490 reach an attack rate of 53% after 2.5 hours of exposure under the simulation boundary conditions

491 reported in section 2.4.2, a quanta emission rate of 341 quanta h^{-1} is needed. Additionally, in this

492 case, such an emission rate occurs at the 92nd percentile of the probability density function (P_q) of

493 an infected subject while singing.

494 Therefore, for both the analyzed cases in the retrospective analyses, the required ER_q values to

495 obtain the documented R_e fall perfectly within the possible values of the emission profiles under

496 consideration (i.e. speaking and singing/speaking loudly in light activity reported in Table 2).

497   Moreover, such emission values incur high individual infection risks as they are around the 90th

498   percentile, i.e. at the percentile maximizing the individual infection risk (R_{max}). Indeed, the R values

499   for the restaurant at Guangzhou and the Skagit Valley choir were 3.2% and 3.7%, respectively –

500   more than one order of magnitude higher than the acceptable risk of 10^{-3}. In these two cases, an

501   individual risk of $< 10^{-3}$ would have been obtained with a probability of infection $P_I = 1.3$-1.4%:

502   such a P_I is not actually achievable by varying and optimizing the room ventilation (e.g.

503    $AER > 100 \, h^{-1}$ would be required), and is achievable only by reducing the exposure time of the
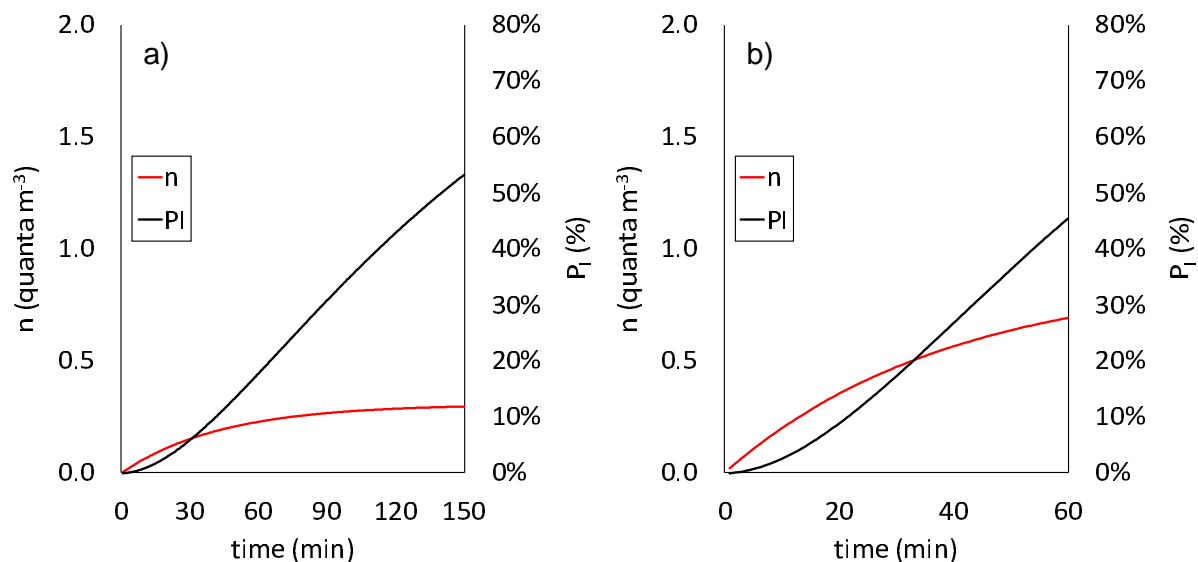
504   susceptible subjects and the quanta emission rates.

505

506   **Figure 5** – Quanta concentration (n) and probability of infection (P_I) evaluated for the retrospective cases

507   applied at the documented outbreaks at (a) the restaurant in Guangzhou and (b) the Skagit Valley choir.

508   To summarize, the retrospective assessment of the two SARS-CoV-2 outbreaks investigated

509   demonstrate that the documented number of infected people can be explained by means of the

510   airborne transmission route; indeed, the most probable of the expected events occurred. The

511   approach and consequent calculation reported here clearly highlights that the explanation of such

512   a high number of infected people does not necessarily require the presence of a superspreader in

513   the environment (i.e. an infected person with the highest viral load, c_v, and infectious dose, c_i), but

514   rather a co-existence of conditions, including emission and exposure parameters, leading to a

515   highly probable event, which can be defined as a "superspreading event".

516

517

518   **References**

519   (1)   Ai, Z. T.; Melikov, A. K. Airborne Spread of Expiratory Droplet Nuclei between the Occupants of

520   Indoor   Environments: A   Review.   *Indoor   Air*   **2018**,   *28*   (4),   500–524.

521   https://doi.org/10.1111/ina.12465.

522   (2)   Holmgren, H.; Ljungström, E.; Almstrand, A.-C.; Bake, B.; Olin, A.-C. Size Distribution of Exhaled

523   Particles in the Range from 0.01 to 2.0µm. *Journal of Aerosol Science* **2010**, *41* (5), 439–446.

524   https://doi.org/10.1016/j.jaerosci.2010.02.011.

525   (3)   van Doremalen, N.; Bushmaker, T.; Morris, D. H.; Holbrook, M. G.; Gamble, A.; Williamson, B. N.;

526   Tamin, A.; Harcourt, J. L.; Thornburg, N. J.; Gerber, S. I.; Lloyd-Smith, J. O.; de Wit, E.; Munster, V. J.

527   Aerosol and Surface Stability of SARS-CoV-2 as Compared with SARS-CoV-1. *N Engl J Med* **2020**.

528   https://doi.org/10.1056/NEJMc2004973.

529   (4)   Ai, Z. T.; Hashimoto, K.; Melikov, A. K. Airborne Transmission between Room Occupants during

530   Short-Term   Events: Measurement   and   Evaluation.   *Indoor   Air*   **2019**,   *29*   (4),   563–576.

531   https://doi.org/10.1111/ina.12557.

532   (5)   Ai, Z. T.; Huang, T.; Melikov, A. K. Airborne Transmission of Exhaled Droplet Nuclei between

533   Occupants in a Room with Horizontal Air Distribution. *Building and Environment* **2019**, *163*, 106328.

534   https://doi.org/10.1016/j.buildenv.2019.106328.

535   (6)   Morawska, L.; Johnson, G. R.; Ristovski, Z. D.; Hargreaves, M.; Mengersen, K.; Corbett, S.; Chao, C. Y.

536   H.; Li, Y.; Katoshevski, D. Size Distribution and Sites of Origin of Droplets Expelled from the Human

537   Respiratory Tract during Expiratory Activities. *Journal of Aerosol Science* **2009**, *40* (3), 256–269.

538   https://doi.org/10.1016/j.jaerosci.2008.11.002.

539   (7)   Morawska, L.; Cao, J. Airborne Transmission of SARS-CoV-2: The World Should Face the Reality.

540   *Environment International* **2020**, *139*, 105730. https://doi.org/10.1016/j.envint.2020.105730.

541   (8)   Chao, C. Y. H.; Wan, M. P.; Morawska, L.; Johnson, G. R.; Ristovski, Z. D.; Hargreaves, M.; Mengersen,

542   K.; Corbett, S.; Li, Y.; Xie, X.; Katoshevski, D. Characterization of Expiration Air Jets and Droplet Size

543   Distributions Immediately at the Mouth Opening. *Journal of Aerosol Science* **2009**, *40* (2), 122–133.

544   https://doi.org/10.1016/j.jaerosci.2008.10.003.

545 (9) Morawska, L. Droplet Fate in Indoor Environments, or Can We Prevent the Spread of Infection?

546   *Indoor Air* **2006**, *16* (5), 335–347. https://doi.org/10.1111/j.1600-0668.2006.00432.x.

547 (10) Hickey, A. J.; Mansour, H. M. *Inhalation Aerosols: Physical and Biological Basis for Therapy, Third*

548   *Edition*; Taylor & Francis Ltd, 2019.

549 (11) Duguid, J. P. The Numbers and the Sites of Origin of the Droplets Expelled during Expiratory

550   Activities. *Edinburgh Medical Journal* **1945**, *LII (II)* (II), 385–401.

551 (12) Jennison, M. W. Atomizing of Mouth and Nose Secretions into the Air as Revealed by High Speed

552   Photography. *Aerobiology* **1942**, *17*, 106–128.

553 (13) Wells, W. F. On Airborne Infection: Study II. Droplets and Droplet Nuclei. *American Journal of*

554   *Epidemiology* **1934**, *20* (3), 611–618. https://doi.org/10.1093/oxfordjournals.aje.a118097.

555 (14) Tang, J. W.; Noakes, C. J.; Nielsen, P. V.; Eames, I.; Nicolle, A.; Li, Y.; Settles, G. S. Observing and

556   Quantifying Airflows in the Infection Control of Aerosol- and Airborne-Transmitted Diseases: An

557   Overview   of   Approaches.   *Journal   of   Hospital   Infection*   **2011**,   *77*   (3),   213–222.

558   https://doi.org/10.1016/j.jhin.2010.09.037.

559 (15) Myatt, T. A.; Minegishi, T.; Allen, J. G.; Macintosh, D. L. Control of Asthma Triggers in Indoor Air with

560   Air Cleaners: A Modeling Analysis. *Environ Health* **2008**, *7*, 43. https://doi.org/10.1186/1476-069X-7-

561   43.

562 (16) Rudnick, S. N.; Milton, D. K. Risk of Indoor Airborne Infection Transmission Estimated from Carbon

563   Dioxide   Concentration.   *Indoor   Air*   **2003**,   *13*   (3),   237–245.   https://doi.org/10.1034/j.1600-

564   0668.2003.00189.x.

565 (17) Sze To, G. N.; Chao, C. Y. H. Review and Comparison between the Wells–Riley and Dose-Response

566   Approaches to Risk Assessment of Infectious Respiratory Diseases. *Indoor Air* **2010**, *20* (1), 2–16.

567   https://doi.org/10.1111/j.1600-0668.2009.00621.x.

568 (18) Wagner, B. G.; Coburn, B. J.; Blower, S. Calculating the Potential for Within-Flight Transmission of

569   Influenza A (H1N1). *BMC Medicine* **2009**, *7* (1), 81. https://doi.org/10.1186/1741-7015-7-81.

570   (19)   Buonanno, G.; Stabile, L.; Morawska, L. Estimation of Airborne Viral Emission: Quanta Emission Rate

571   of   SARS-CoV-2   for   Infection   Risk   Assessment.   *Environment   International*   **2020**.

572   https://doi.org/10.1101/2020.04.12.20062828.

573   (20)   Gammaitoni, L.; Nucci, M. C. Using a Mathematical Model to Evaluate the Efficacy of TB Control

574   Measures. *Emerging Infectious Diseases* **1997**, 335–342.

575   (21)   Riley, C.; Murphy, G.; Riley, R. L. Airborne Spread of Measles in a Suburban Elementary School.

576   *American journal of epidemiology* **1978**, No. 107, 431–432.

577   (22)   Hammersley, J. M.; Handscomb, D. C. *Monte Carlo Methods*; Chapman and Hall: London & New

578   York, 1964.

579   (23)   Pan, Y.; Zang, D.; Yang, P.; Poon, L. M.; Wang, Q. Viral Load of SARS-CoV-2 in Clinical Samples Yang

580   Pan Daitao Zhang Peng Yang Leo L M Poon Quanyi Wang. *The Lancet* **2020**.

581   (24)   Rothe, C.; Schunk, M.; Sothmann, P.; Bretzel, G.; Froeschl, G.; Wallrauch, C.; Zimmer, T.; Thiel, V.;

582   Janke, C.; Guggemos, W.; Seilmaier, M.; Drosten, C.; Vollmar, P.; Zwirglmaier, K.; Zange, S.; Wölfel,

583   R.; Hoelscher, M. Transmission of 2019-NCoV Infection from an Asymptomatic Contact in Germany.

584   *N Engl J Med* **2020**, *382* (10), 970–971. https://doi.org/10.1056/NEJMc2001468.

585   (25)   To, K. K.-W.; Tsang, O. T.-Y.; Leung, W.-S.; Tam, A. R.; Wu, T.-C.; Lung, D. C.; Yip, C. C.-Y.; Cai, J.-P.;

586   Chan, J. M.-C.; Chik, T. S.-H.; Lau, D. P.-L.; Choi, C. Y.-C.; Chen, L.-L.; Chan, W.-M.; Chan, K.-H.; Ip, J. D.;

587   Ng, A. C.-K.; Poon, R. W.-S.; Luo, C.-T.; Cheng, V. C.-C.; Chan, J. F.-W.; Hung, I. F.-N.; Chen, Z.; Chen,

588   H.; Yuen, K.-Y. Temporal Profiles of Viral Load in Posterior Oropharyngeal Saliva Samples and Serum

589   Antibody Responses during Infection by SARS-CoV-2: An Observational Cohort Study. *The Lancet*

590   *Infectious Diseases* **2020**. https://doi.org/10.1016/S1473-3099(20)30196-1.

591   (26)   Woelfel, R.; Corman, V. M.; Guggemos, W.; Seilmaier, M.; Zange, S.; Mueller, M. A.; Niemeyer, D.;

592   Vollmar, P.; Rothe, C.; Hoelscher, M.; Bleicker, T.; Bruenink, S.; Schneider, J.; Ehmann, R.;

593   Zwirglmaier, K.; Drosten, C.; Wendtner, C. Clinical Presentation and Virological Assessment of

594   Hospitalized Cases of Coronavirus Disease 2019 in a Travel-Associated Transmission Cluster. *medRxiv*

595   **2020**, 2020.03.05.20030502. https://doi.org/10.1101/2020.03.05.20030502.

596   (27)   Watanabe, T.; Bartrand, T. A.; Weir, M. H.; Omura, T.; Haas, C. N. Development of a Dose-Response

597   Model for SARS Coronavirus. *Risk Anal* **2010**, *30* (7), 1129–1138. https://doi.org/10.1111/j.1539-

598   6924.2010.01427.x.

599   (28)   Yang, W.; Marr, L. C. Dynamics of Airborne Influenza A Viruses Indoors and Dependence on

600   Humidity. *PLOS ONE* **2011**, *6* (6), e21481. https://doi.org/10.1371/journal.pone.0021481.

601   (29)   Chatoutsidou, S. E.; Lazaridis, M. Assessment of the Impact of Particulate Dry Deposition on Soiling

602   of Indoor Cultural Heritage Objects Found in Churches and Museums/Libraries. *Journal of Cultural*

603   *Heritage* **2019**, *39*, 221–228. https://doi.org/10.1016/j.culher.2019.02.017.

604   (30)   Haas, C. N. Estimation of Risk Due to Low Doses of Microorganisms: A Comparison of Alternative

605   Methodologies. *Am   J   Epidemiol* **1983**, *118*   (4),   573–582.

606   https://doi.org/10.1093/oxfordjournals.aje.a113662.

607   (31)   Cotruvo, J. A. Drinking Water Standards and Risk Assessment. *Regul Toxicol Pharmacol* **1988**, *8* (3),

608   288–299. https://doi.org/10.1016/0273-2300(88)90016-5.

609   (32)   World Health Organization. *Guidelines for Drinking-Water Quality - 4th Edition*; WHO Regional Office

610   for Europe, 2011.

611   (33)   Toner, G. *Innovation, Science, Environment 08/09*; McGill-Queen's University Press, 2008.

612   (34)   Lu, J.; Gu, J.; Li, K.; Xu, C.; Su, W.; Lai, Z.; Zhou, D.; Yu, C.; Xu, B.; Yang, Z. COVID-19 Outbreak

613   Associated with Air Conditioning in Restaurant, Guangzhou, China, 2020. *Emerg Infect Dis* **2020**, *26*

614   (7). https://doi.org/10.3201/eid2607.200764.

615   (35)   Hamner, L.; Dubbel, P.; Capron, I.; Ross, A.; Jordan, A.; Lee, J.; Lynn, J.; Ball, A.; Narwal, S.; Russell, S.;

616   Patrick, D.; Leibrand, H. High SARS-CoV-2 Attack Rate Following Exposure at a Choir Practice - Skagit

617   County, Washington, March 2020. *Morbidity and Mortality Weekly Report* **2020**, *69*.

618   (36)   Asadi, S.; Wexler, A. S.; Cappa, C. D.; Barreda, S.; Bouvier, N. M.; Ristenpart, W. D. Aerosol Emission

619   and Superemission during Human Speech Increase with Voice Loudness. *Scientific Reports* **2019**, *9*

620   (1), 2348. https://doi.org/10.1038/s41598-019-38808-z.

621　(37)　European Committee for Standardisation. UNI EN 15251 - Indoor Environmental Input Parameters

622　　　for Design and Assessment of Energy Performance of Buildings Addressing Indoor Air Quality,

623　　　Thermal Environment, Lighting and Acoustics. **2008**.

624